



# Macroscopic and Microstructural Aspects of the Transformation Behavior in a Polycrystalline NiTi Shape Memory Alloy

*Othmane Benafan, Ronald D. Noebe, Santo A. Padula II, Bradley A. Lerch, and Glen S. Bigelow  
Glenn Research Center, Cleveland, Ohio*

*Darrell J. Gaydos  
Ohio Aerospace Institute, Brook Park, Ohio*

*Anita Garg  
University of Toledo, Toledo, Ohio*

*Ke An  
Oak Ridge National Laboratory, Oak Ridge, Tennessee*

*Raj Vaidyanathan  
University of Central Florida, Orlando, Florida*

## NASA STI Program . . . in Profile

Since its founding, NASA has been dedicated to the advancement of aeronautics and space science. The NASA Scientific and Technical Information (STI) program plays a key part in helping NASA maintain this important role.

The NASA STI Program operates under the auspices of the Agency Chief Information Officer. It collects, organizes, provides for archiving, and disseminates NASA's STI. The NASA STI program provides access to the NASA Aeronautics and Space Database and its public interface, the NASA Technical Reports Server, thus providing one of the largest collections of aeronautical and space science STI in the world. Results are published in both non-NASA channels and by NASA in the NASA STI Report Series, which includes the following report types:

- **TECHNICAL PUBLICATION.** Reports of completed research or a major significant phase of research that present the results of NASA programs and include extensive data or theoretical analysis. Includes compilations of significant scientific and technical data and information deemed to be of continuing reference value. NASA counterpart of peer-reviewed formal professional papers but has less stringent limitations on manuscript length and extent of graphic presentations.
- **TECHNICAL MEMORANDUM.** Scientific and technical findings that are preliminary or of specialized interest, e.g., quick release reports, working papers, and bibliographies that contain minimal annotation. Does not contain extensive analysis.
- **CONTRACTOR REPORT.** Scientific and technical findings by NASA-sponsored contractors and grantees.

- **CONFERENCE PUBLICATION.** Collected papers from scientific and technical conferences, symposia, seminars, or other meetings sponsored or cosponsored by NASA.
- **SPECIAL PUBLICATION.** Scientific, technical, or historical information from NASA programs, projects, and missions, often concerned with subjects having substantial public interest.
- **TECHNICAL TRANSLATION.** English-language translations of foreign scientific and technical material pertinent to NASA's mission.

Specialized services also include creating custom thesauri, building customized databases, organizing and publishing research results.

For more information about the NASA STI program, see the following:

- Access the NASA STI program home page at <http://www.sti.nasa.gov>
- E-mail your question to [help@sti.nasa.gov](mailto:help@sti.nasa.gov)
- Fax your question to the NASA STI Information Desk at 443-757-5803
- Phone the NASA STI Information Desk at 443-757-5802
- Write to:  
STI Information Desk  
NASA Center for AeroSpace Information  
7115 Standard Drive  
Hanover, MD 21076-1320



# Macroscopic and Microstructural Aspects of the Transformation Behavior in a Polycrystalline NiTi Shape Memory Alloy

*Othmane Benafan, Ronald D. Noebe, Santo A. Padula II, Bradley A. Lerch, and Glen S. Bigelow  
Glenn Research Center, Cleveland, Ohio*

*Darrell J. Gaydosch  
Ohio Aerospace Institute, Brook Park, Ohio*

*Anita Garg  
University of Toledo, Toledo, Ohio*

*Ke An  
Oak Ridge National Laboratory, Oak Ridge, Tennessee*

*Raj Vaidyanathan  
University of Central Florida, Orlando, Florida*

National Aeronautics and  
Space Administration

Glenn Research Center  
Cleveland, Ohio 44135

## Acknowledgments

Funding from the NASA Fundamental Aeronautics Program, Aeronautical Sciences and Fixed Wing Projects is gratefully acknowledged. The authors thank D.E. Nicholson and H.D. Skorpenske for technical support and helpful discussions. This work has benefited from the use of the Spallation Neutron Source at Oak Ridge National Laboratory, which is funded by the Division of Scientific User Facilities, Office of Basic Energy Sciences, U.S. Department of Energy under Contract DE-AC05-00OR22725 with UT-Battelle, LLC.

This work was sponsored by the Fundamental Aeronautics Program  
at the NASA Glenn Research Center.

*Level of Review:* This material has been technically reviewed by technical management.

Available from

NASA Center for Aerospace Information  
7115 Standard Drive  
Hanover, MD 21076-1320

National Technical Information Service  
5301 Shawnee Road  
Alexandria, VA 22312

Available electronically at <http://www.sti.nasa.gov>

# Macroscopic and Microstructural Aspects of the Transformation Behavior in a Polycrystalline NiTi Shape Memory Alloy

Othmane Benafan, Ronald D. Noebe, Santo A. Padula II, Bradley A. Lerch, and Glen S. Bigelow  
National Aeronautics and Space Administration  
Glenn Research Center  
Cleveland, Ohio 44135

Darrell J. Gaydos  
Ohio Aerospace Institute  
Brook Park, Ohio 44142

Anita Garg  
University of Toledo  
Toledo, Ohio 43606

Ke An  
Oak Ridge National Laboratory  
Oak Ridge, Tennessee 37831

Raj Vaidyanathan  
University of Central Florida  
Orlando, Florida 32816

## Abstract

The mechanical and microstructural behavior of a polycrystalline Ni<sub>49.9</sub>Ti<sub>50.1</sub> (at.%) shape memory alloy was investigated as a function of temperature around the transformation regime. The bulk macroscopic responses, measured using *ex situ* tensile deformation and impulse excitation tests, were compared to the microstructural evolution captured using *in situ* neutron diffraction. The onset stress for inelastic deformation and dynamic Young's modulus were found to decrease with temperature, in the martensite regime, reaching a significant minimum at approximately 80 °C followed by an increase in both properties, attributed to the martensite to austenite transformation. The initial decrease in material compliance during heating affected the ease with which martensite reorientation and detwinning could occur, ultimately impacting the stress for inelastic deformation prior to the start of the reverse transformation.

## 1.0 Introduction

The integration of shape memory alloys (SMAs) in high work output, solid-state actuators has been a topic of major interest in recent years. The functional properties of SMAs have been shown to favorably exceed those of conventional actuators leading to new solutions and capabilities for a number of potential applications (Refs. 1 and 2). However, the transition from functional properties to functional devices in large scale commercial applications has been hindered by concerns about dimensional/thermal stability and the long term durability of the SMAs. These concerns stem from the limited knowledge base for these unique materials and the governing transformation and deformation processes. Thus, an understanding of these key issues will further the maturation and implementation of SMAs in actuator applications.

Among many classes of SMAs, near equiatomic NiTi has been the material of choice for most research and development tasks. Near equiatomic NiTi exhibits large actuation strains (exceeding 4%) associated with the phase transformation between the higher temperature B2 austenite and the lower

temperature B19' martensite phases. Recently, the deformation mechanisms in these two phases have been studied in detail using *in situ* neutron diffraction techniques (Refs. 3 to 5), more clearly identifying and mapping the various deformation processes and regimes. However, more work is required to fully understand the material behavior during the temperature excursion in an actuation cycle.

Thus, the objective of this study was to investigate the influence of temperature on both the deformation and transformation behavior of bulk polycrystalline NiTi through the transformation regime. Combined macroscopic and atomic-scale experiments were performed for that purpose. Macroscopic experiments consisted of (i) uniaxial tensile loading at different temperatures to identify the apparent onset of inelastic deformation, and (ii) impulse excitation of vibration tests to determine the temperature dependence of the dynamic Young's modulus. Since NiTi undergoes a diffusionless phase change during the martensitic transformation, most conventional characterization tools are of limited utility in determining microstructural details over this range. However, through the unique capabilities of *in situ* neutron diffraction, it is possible to determine the effect of stress and temperature on the mechanical response of the alloy while simultaneously following changes in the alloy's internal state and microstructure.

## 2.0 Material and Experimental Procedures

The material used was a binary Ni<sub>49.9</sub>Ti<sub>50.1</sub> (at.%) alloy produced by Special Metals, New Hartford, New York (now SAES Smart Materials). Various physical and thermomechanical properties of this particular alloy are available in the literature (Refs. 4 to 13). Test specimens were machined from the hot-rolled/hot-drawn and hot-straightened 10 mm diameter rod (as-received condition). Differential scanning calorimetry (DSC) measurements were performed on the as-received material using a standard heating/cooling rate of 10 °C/min, and the martensite start ( $M_s$ ), martensite finish ( $M_f$ ), austenite start ( $A_s$ ) and austenite finish ( $A_f$ ) temperatures were found to be 75, 47, 89 and 113 °C  $\pm$  2 °C, respectively.

*Ex situ* thermomechanical tests were performed on an 810 MTS servohydraulic load frame. Prior to mechanical loading, the specimens were thermally cycled in the load frame under no-load between room temperature and 200 °C at a rate of 20 °C/min while measuring strain. In addition to determining the stress-free transformation temperatures, the thermal cycling process was used to relieve any residual stresses in the samples due to processing or machining and to ensure a self-accommodated martensite starting structure. Adopting the ASTM Standard F2082–06 (Ref. 14),  $M_s$ ,  $M_f$ ,  $A_s$  and  $A_f$  temperatures were measured using the tangent intercept method and were found to be 71, 55, 92, and 105  $\pm$  2 °C, respectively, consistent with the temperatures determined by DSC. The cylindrical dogbone specimens (5 mm gage diameter) were subsequently deformed in uniaxial tension to 18% in strain control at a rate of  $1 \times 10^{-4}$  sec<sup>-1</sup> at temperatures between 30 and 230 °C (Figure 1(a)).

Dynamic Young's modulus testing (Figure 2) was performed using the impulse excitation of vibration method as per ASTM Standard E1876 (Ref. 15). Rods of circular cross section ( $\phi = 4.95 \times l = 50.2$  mm) and rectangular bars with two different geometries (4.9 $\times$ 4.9 $\times$ 50 mm and 3 $\times$ 4 $\times$ 50 mm) were heated in a furnace in an argon atmosphere at rates of 200 and 765 °C/hr (Figure 2). Tests were conducted between room temperature and 200 °C with data sampled every 2 °C.

*In situ* neutron diffraction experiments were performed on the engineering materials diffractometer (VULCAN) at the Spallation Neutron Source (SNS), Oak Ridge National Laboratory (ORNL). A detailed description of the instrument can be found elsewhere (Ref. 16 and 17). In short, the incident neutron beam impinges on the sample with the loading axis positioned at 45° relative to the beam, with diffraction data collected simultaneously by the two scintillation detectors positioned on either side of the incident beam path at  $\pm 90^\circ$  at a distance of 2 m from the sample. The *in situ* experimental setup is shown in Figure 3. An incident beam size of 3 $\times$ 4 mm and a chopper speed of 20 Hz at 1 MW nominal source power were used for the diffraction measurements. Cylindrical dogbone samples (5 mm gage diameter) were thermally cycled between room temperature and 230 °C while maintaining zero stress. Neutron data were collected continuously and in intervals while heating and cooling at a rate of 200 °C/hr. Neutron diffraction data was analyzed using the event mode data reduction software VDRIVE (Ref. 18).

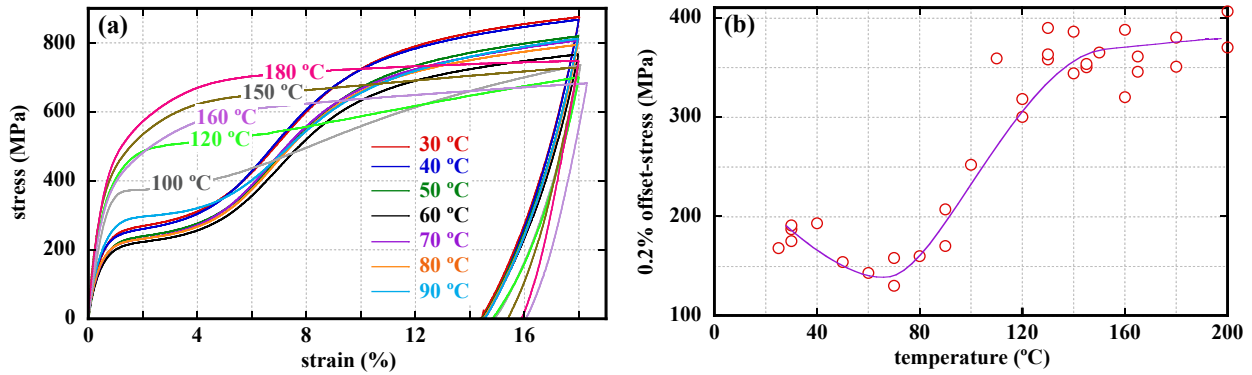
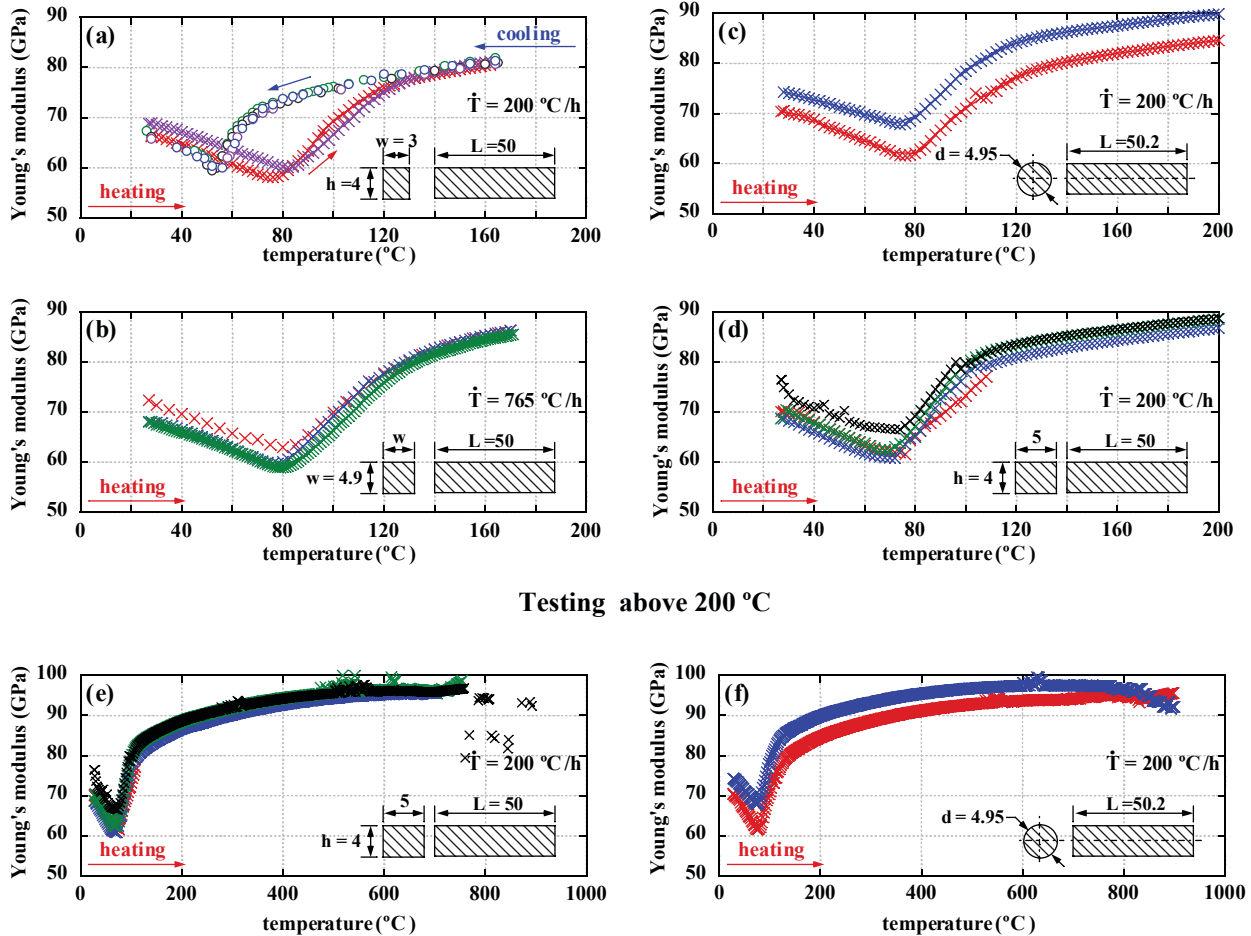


Figure 1.—(a) Tensile stress-strain responses of  $\text{Ni}_{49.9}\text{Ti}_{50.1}$  samples deformed isothermally to 18% strain at temperatures between 30 and 200 °C. (b) 0.2% offset yield stress behavior of  $\text{Ni}_{49.9}\text{Ti}_{50.1}$  determined in tension as a function of temperature.



Testing above 200 °C

Figure 2.—Dynamic Young's modulus for  $\text{Ni}_{49.9}\text{Ti}_{50.1}$  as a function of temperature for (a) 4.9×4.9×50 mm rectangular bar using a heating/cooling rate of 200 °C/hr, (b) 3×4×50 mm rectangular bar using a heating rate of 765 °C/hr, (c)  $\phi = 4.95 \times l = 50.2$  mm rod of circular cross section using a heating rate of 200 °C/hr, (d) 5×4×50 mm rectangular bar using a heating rate of 200 °C/hr, and (e) and (f) modulus data above 200 °C. (Different symbols correspond to multiple samples that were tested under the same condition).

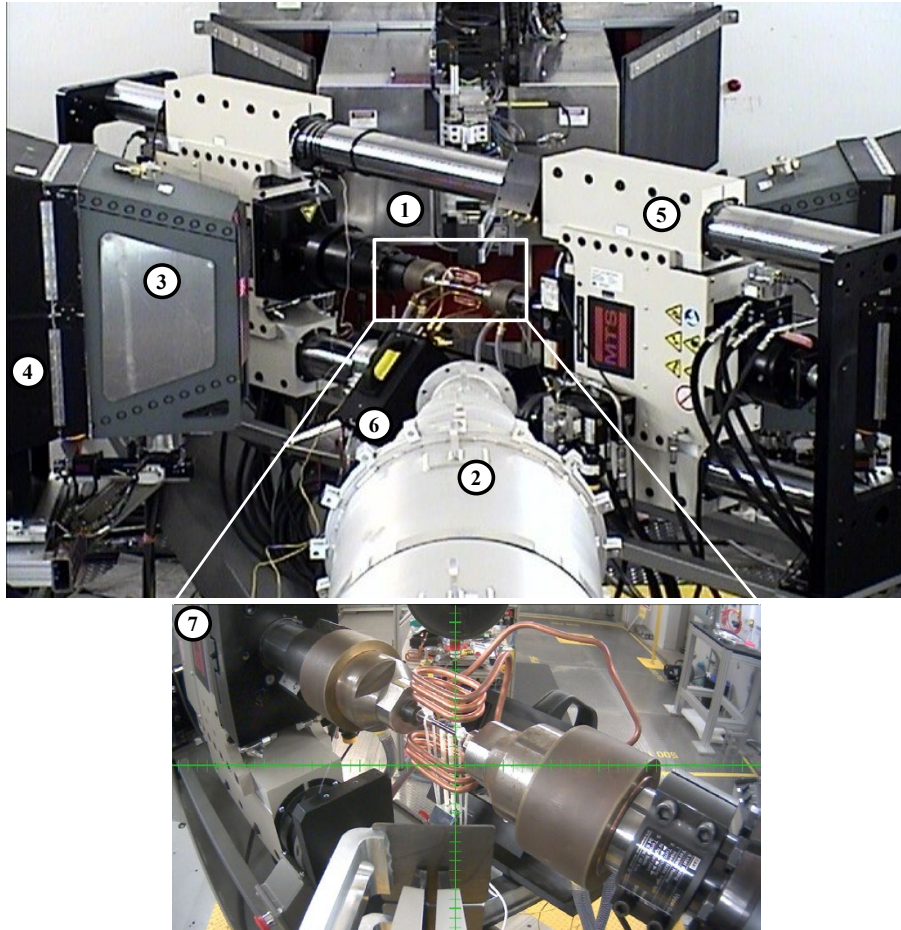


Figure 3.—VULCAN experimental setup for *in situ* neutron diffraction measurement. 1. Incident beam, 2. beam-stop, 3. collimator, 4. Detector shielding box, 5. axial-torsional load frame, 6. induction heater, 7. NiTi sample mounted between water cooled grips, parallel induction coils and high temperature extensometer (viewed from the upstream of neutron beam).

### 3.0 Results and Discussion

The macroscopic stress-strain response of the  $\text{Ni}_{49.9}\text{Ti}_{50.1}$  alloy is shown in Figure 1(a) for samples deformed isothermally to 18% strain over a wide range of temperatures. The 18% strain level was sufficient to reveal multiple deformation regimes at each temperature as previously determined for this material by Benafan (Refs. 3 and 5) and Stebner (Ref. 4). In the martensite phase, the following deformation regimes were observed with increasing stress: elastic deformation plus martensite reorientation, transformation twinning processes, deformation twinning and slip (Refs. 3 and 5). Above  $A_s$ , deformation consisted of elastic, stress-induced martensite, and plastic deformation of austenite by dislocation mediated processes and twinning (Ref. 3). Unlike the elastic response of the austenite phase, which is linear up to about 350 MPa, the apparent martensitic elastic region showed non-linear behavior due to the simultaneous operation, at very low stresses, of martensite reorientation/detwinning mechanisms (Ref. 7). As a result, the macroscopic measurements from extensometry furnished deflated values for Young's moduli, as discussed later in this paper. With increasing strain, the martensite tensile curves exhibited a stress plateau or region of low hardening rate that was dependent on temperature. This behavior was discernible in samples tested between room temperature and 90 °C where the material is martensitic ( $T < A_s$ ), and gradually transitioned into a more conventional hardening behavior at temperatures above  $A_f$ .

The onset of the macroscopic non-linear deformation was measured using a 0.2% strain offset criterion and the results as a function of temperature are summarized in Figure 1(b). Additional tensile tests (not shown in Figure 1(a)) were performed between room temperature and 200 °C to better define the statistical fit in Figure 1(b). Although the initial B19' response exhibits nonlinear behavior, a 0.2% offset criteria was still used over a region of best linear fit between 0 and 150 MPa. The onset of inelastic deformation (generally referred to as 'yield') in the martensite phase is dominated by reorientation and detwinning mechanisms and was found to decrease with increasing test temperature, reaching an averaged minimum value of 140 MPa between 65 and 80 °C (Figure 1(b)). The onset stress then sharply increased in the two-phase region and reached near saturation (with a still slightly positive slope) at 350 MPa near 130 °C. Inelastic deformation over this temperature range (~90 to 130 °C), which includes the B19'→B2 phase transition, is attributed to the nearly concurrent operation of stress-induced martensite and plastic deformation (Ref. 3).

A similar trend with temperature was also obtained in the dynamic Young's modulus data obtained from the impulse excitation of vibration tests as illustrated in Figure 2. This data was generated using different sample geometries and temperature rates, but always yielded similar results. Consistently, the average dynamic modulus of martensite at room temperature was about 70 GPa, but decreased with increasing temperature with an average minimum value of 60 GPa at ~80 °C. The modulus then increased through the two-phase region reaching an average value of 78 GPa at 130 °C. The strong temperature dependence in the two-phase region is due to the effective modulus of the constantly changing volume fractions of martensite and austenite with increasing temperature. Note that the modulus in the austenite phase (> 130 °C) did not saturate at a unique value, consistent with the yield behavior shown in Figure 1(b), but continued to gradually increase with temperature. These results suggest that martensite is still present at some level in the material at temperatures above 130 °C, even though the  $A_f$  determined by DSC was only 113 °C. Also included in Figure 2(a) is the dynamic modulus data measured during cooling. In addition to the hysteresis associated with the forward transformation, the minimum modulus obtained during cooling was identical to that during heating and averaged 60 GPa.

Apparent elastic moduli were also determined from the initial slopes of the tensile stress-strain curves for each phase. Using this technique, the modulus was 50 GPa for the martensite phase at room temperature and was 74 GPa for austenite at 165 °C. Both values are lower than the dynamic moduli, which were 70 and 83 GPa, respectively. The differences stem from the early onset of inelastic deformation as the tensile load was applied during mechanical testing (i.e., reorientation and detwinning in the martensite phase and the presence of stress-induced martensite in the austenite phase), resulting in deflated modulus values, particularly at lower temperatures (Refs. 7 and 19). However, it is important to note that even the modulus values determined by the dynamic technique resulted in deflated values compared to the "true" values for this material. The "true" elastic modulus of martensite is higher than that of the austenite as was reported in previous studies, which is not revealed by the current macroscopic methods. It was reported that the averaged, "true" B19' Young's modulus of this alloy was 134 GPa (Ref. 7), measured using *in situ* neutron diffraction, 101 GPa from instrumented indentation (Ref. 19), and 122.3 GPa determined using *ab initio* calculations (Ref. 20). The higher martensite modulus was also reported for a single crystal, superelastic NiTi determined through repeated unloading experiments in compression (Ref. 21). Consequently, the macroscopic moduli for the studied NiTi alloy investigated in this study are considered the apparent moduli since inelastic deformation mechanisms, namely martensite reorientation/detwinning, can reduce the "true" elastic modulus value.

*In situ* neutron diffraction was used to track detailed microstructural changes during the transformation process. The strain-temperature responses measured *ex situ* at NASA Glenn Research Center and *in situ* at VULCAN during the neutron diffraction experiments are compared in Figure 4. The data correspond to a no-load thermal cycle and are essentially identical, confirming the consistency in temperature measurement between the two facilities. From Rietveld refinement of the neutron data, the B19' martensite exists in the self-accommodated state with best-fit lattice parameters of  $a=2.903 \text{ \AA}$ ,  $b=4.64 \text{ \AA}$ ,  $c=4.12 \text{ \AA}$ ,  $\alpha=\beta=90^\circ$  and  $\gamma=97.63^\circ$  that transforms to B2 austenite with a best-fit lattice parameter of  $a=3.03 \text{ \AA}$ . The output of the refined B19' and B2 neutron spectra under no load at RT and 450 °C, respectively are shown in Figure 5.

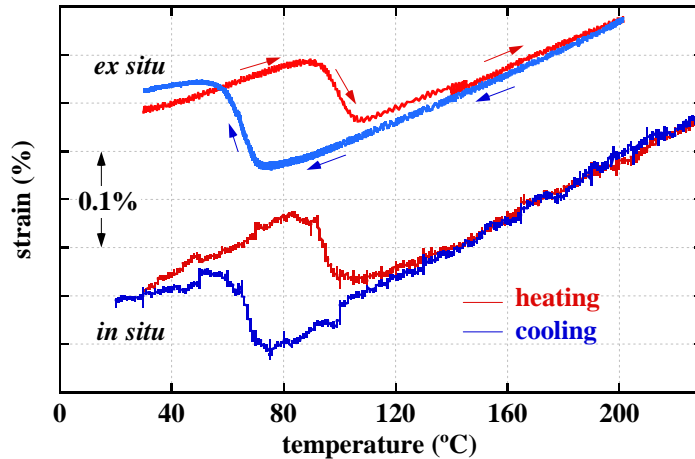


Figure 4.—Macroscopic strain-temperature response from *ex situ* and *in situ* no-load thermal cycle of Ni<sub>49.9</sub>Ti<sub>50.1</sub>.

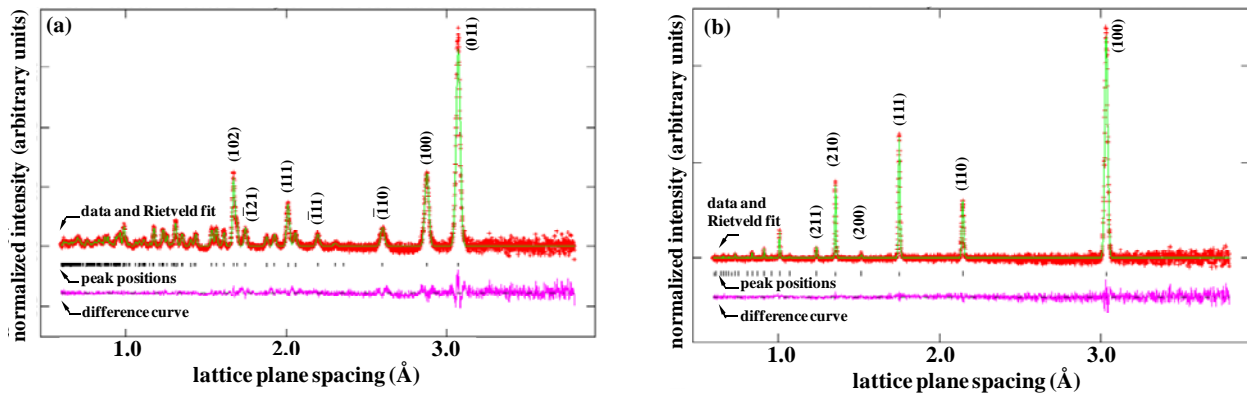


Figure 5.—Rietveld refinement for NiTi with diffracting lattice planes parallel to the loading axis with no applied load. (a) Monoclinic martensite at 30 °C and (b) cubic austenite at 230 °C. The measured data are indicated by cross-marks and the calculated profile is indicated by the solid line. The tick-marks below the profile pattern indicate the reflections. The lower curve is the difference between the measurement and refinement.

Neutron spectra were collected continuously during temperature cycling and for visualization purposes the data are displayed as contour plots in Figure 6(a) for the heating cycle and in Figure 6(b) for the cooling cycle. These spectra are from lattice planes with their plane normals parallel to the sample axis. The dashed lines across the contour plots indicate the start and end of the phase transformation as obtained by the tangent intercept method from the macroscopic strain-temperature data in Figure 4, which are also similar to the DSC values. The diffraction patterns acquired during heating (Figure 6(a)), however, clearly showed the austenite phase starting to form at  $\sim 75$  °C, which is much lower than the macroscopically determined  $A_s$  of 92 °C or DSC measured  $A_s$  of 86 °C. This lower  $A_s^{neutron}$  of  $\sim 75$  °C explains the minima reached between 65 and 80 °C in both the yielding characteristics (Figure 1(b)) and in the dynamic modulus data (Figure 2), which occur below the  $A_s$  temperature as determined by the bulk methods discussed above. Furthermore, the spectra also revealed that even for no-load cycling, the  $(\bar{1}10)_M$  martensite reflections, although weak, were retained in the microstructure after the  $A_f$  and did not completely transform even at 230 °C. In contrast, the phase transformation start and finish temperatures determined from Figure 6(b) on cooling were nearly identical to the bulk measured  $M_s$  and  $M_f$ .

The broader transformation range during heating can be attributed to the elastic (Ref. 7) and thermal (Ref. 8) anisotropy that arises from the symmetry of monoclinic martensite. The highly anisotropic and low symmetry martensite in polycrystalline form gives rise to internal constraints between variants, which facilitate the early transformation of some variants and significantly hinder others. As a result, a broader

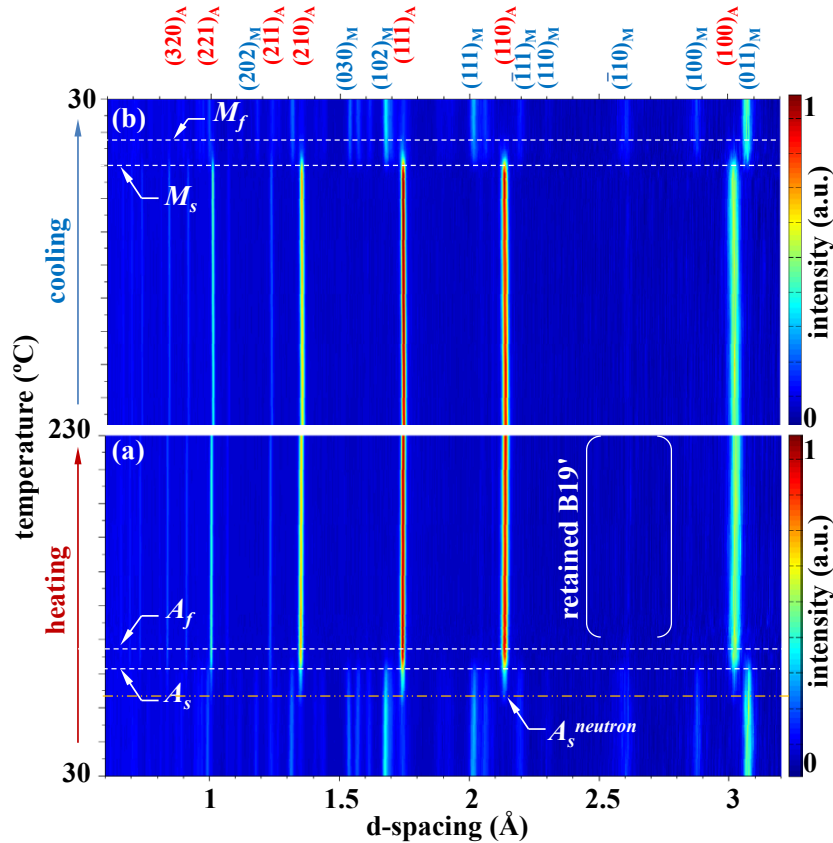


Figure 6.—Normalized neutron diffraction contour plots as a function of d-spacing and temperature during (a) heating and (b) cooling. Subscripts ‘A’ and ‘M’ refer to austenite and martensite, respectively.

transformation range is detected microscopically, especially skewed to higher temperatures, as all martensite variants under an imposed internal stress have to transform to a single unique austenite structure. In contrast, during cooling the higher symmetry austenite phase is relatively isotropic in nature resulting in a well-defined (macroscopically and microscopically) and narrow transformation range. The lack of internal constraints in this case allows the austenite structure to transform to multiple variants of martensite to form a self-accommodated martensite structure with matching macroscopic and microscopic  $M_s$  and  $M_f$  transformation temperatures. It should be noted that there was no evidence of retained austenite during the forward transformation on cooling.

To further support this hypothesis, peak intensities were measured at discrete temperatures. The normalized integrated intensities associated with specific martensite (open symbols) and austenite (solid symbols) reflections as a function of temperature through the transformation are shown in Figure 7(a) to (b). Single peaks were fit to determine these intensities for various representative reflections of each phase with plane normals parallel to the sample axis. Just above room temperature and well below the macroscopically determined  $A_s$ , the intensities vary with temperature, indicative of the preferential transformation of selected martensite variants associated with changes in the material’s compliance (as shown in Figure 2). This preferential transformation is indicated by the increase in  $(100)_M$  and  $(030)_M$  orientations at the expense of  $(002)_M$  and  $(011)_M$ .

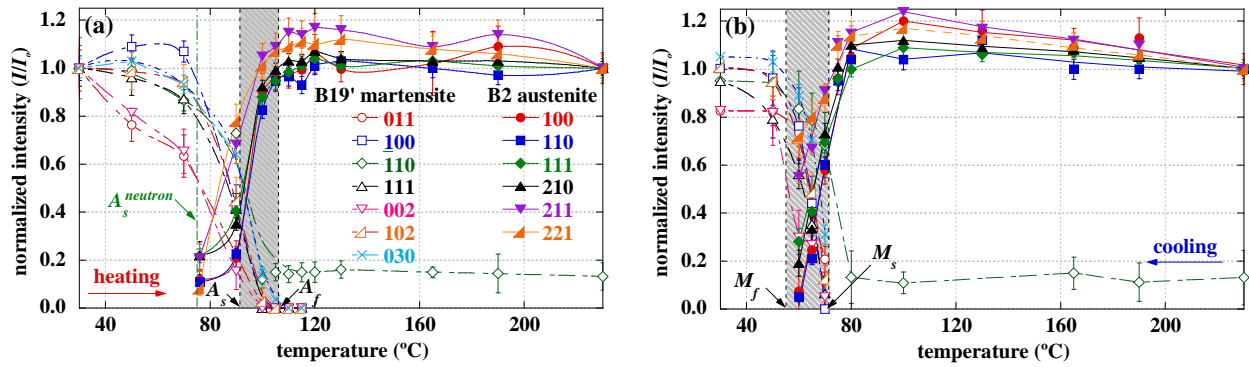


Figure 7.—Normalized intensities from lattice planes with plane normals parallel to the sample axis as a function of temperature during (a) heating and (b) cooling. The shaded vertical bands indicate the start and finish of the transformation as determined from the macroscopic strain-temperature measurements.

The significant intensity evolution of the martensite phase above 75 °C is mainly due to the changes in the martensite/austenite volume fractions and not due to additional texturing of the martensite from variant reorientation. The internal constraints associated with the anisotropy and symmetry force some variants to transform to austenite as early as 75 °C. As the temperature approaches  $A_f$ , most of the B19' intensities decrease, approaching zero between  $A_s$  and  $A_f$ . Simultaneously, the B2 intensities increase, starting around the same temperature range where the slopes for the yield and dynamic modulus data change sign. No significant evolution in texture was observed for the austenite phase, but traces of retained  $(\bar{1}10)_M$  martensite were still detectable above  $A_f$ . On cooling, most of the intensity changes took place in the transformation band and no significant intensity changes were observed below  $M_f$ . These discrete intensity measurements further confirm the broader transformation band on heating with differences between the macroscopic and microscopic  $A_s$  and  $A_f$  and the narrower transformation region with similar  $M_s$  and  $M_f$  obtained from both macro and micro measurements.

The neutron diffraction data explains the minima reached in the yield data (Figure 1(b)) and in the dynamic modulus data (Figure 2), since the actual  $A_s^{neutron}$  for this material takes place at ~75 °C. The  $A_s$  was overestimated at ~90 °C based on the strain-temperature data and the DSC measurements. Furthermore, it is clear that martensite is retained in the microstructure at temperatures well above the bulk  $A_f$ . The bulk transformation temperatures were not consistent with those determined microstructurally during the reverse transformation on heating but matched the measurements during the forward transformation on cooling, for the same reasons presented previously.

## 4.0 Summary and Conclusions

The effect of temperature on the transformation behavior of polycrystalline Ni<sub>49.9</sub>Ti<sub>50.1</sub> (at.%) was investigated. Based on the combined macroscopic and microstructural data presented, the following conclusions were drawn;

- 1) The yield or onset stress for inelastic deformation of NiTi was determined in a temperature range from 30 to 200 °C. Three major deformation regimes were identified as a function of temperature: i) from 30 to ~75 °C, where the material is fully martensitic; yield stress decreased gradually with temperature and was dominated by reorientation and detwinning of the martensite, ii) from 80 to 130 °C, which traverses the martensite-to-austenite transformation region; yield increased sharply with temperature and was controlled by the formation of stress-induced martensite (that occurred almost concurrently with plastic deformation of the austenite phase), and iii) at temperatures above 130 °C, which is above the macroscopic  $A_f$  temperature (though trace amounts of retained martensite are still present); yield stress increased very gradually with increasing temperature to at least 200 °C, presumably due to the continued

presence of trace amounts of retained martensite and its effect on deformation behavior, though significant scatter was observed in the mechanical test data.

2) The dynamic Young's modulus determined from the impulse excitation of vibration method was found to decrease with temperature reaching a minimum of 60 GPa at  $\sim 80$  °C. This change in compliance was responsible for the corresponding decrease in yield stress over this same temperature range by making it easier for martensite reorientation/detwinning to occur. This was followed by an increase in modulus with temperature to 80 GPa at temperatures beyond 130 °C, which was a reflection of the constantly changing martensite to austenite volume fractions with increasing temperature.

3) Transformation temperatures during the reverse transformation measured from strain-temperature and DSC data were found to differ from the actual onset of transformation as seen in neutron spectra and supported by the yield and dynamic modulus data, which suggested an actual austenite start temperature of  $\sim 75$  °C. This was attributed to the anisotropy that arises from the symmetry of monoclinic martensite and the associated internal constraints between variants. A small amount of retained martensite was found in the microstructure at temperature as high as 230 °C. In contrast, the transformation temperatures during the forward transformation determined by neutron diffraction were consistent with those determined by DSC and strain-temperature data since the elastic anisotropy of the high symmetry austenite is negligible. Furthermore, no evidence of retained austenite was found in the current study.

## References

1. S. Hirose, K. Ikuta, Y. Umetani, *Adv. Robot.* 3 (1989) 3-16.
2. C. Mavroidis, *Res. Nondestr. Eval.* 14 (2002) 1-32.
3. O. Benafan, Ph.D. dissertation, University of Central Florida, Orlando, 2012.
4. A.P. Stebner, Ph.D. dissertation, Northwestern University, Evanston, 2012.
5. O. Benafan, S.A. Padula II, R.D. Noebe, T.A. Sisneros, R. Vaidyanathan, *J. Appl. Phys.* 112 (2012) 093510.
6. S. Manchiraju, D. Gaydosh, O. Benafan, R. Noebe, R. Vaidyanathan, P.M. Anderson, *Acta Mater.* 59 (2011) 5238-5249.
7. S. Qiu, B. Clausen, S.A. Padula II, R.D. Noebe, R. Vaidyanathan, *Acta Mater.* 59 (2011) 5055-5066.
8. S. Qiu, V.B. Krishnan, S.A. Padula II, R.D. Noebe, D.W. Brown, B. Clausen, R. Vaidyanathan, *Appl. Phys. Lett.* 95 (2009) 141906.
9. S. Padula II, S. Qiu, D. Gaydosh, R. Noebe, G. Bigelow, A. Garg, R. Vaidyanathan, *Metall. Mater. Trans. A* 43 (2012) 4610-4621.
10. O. Benafan, *Deformation and Transformation Processes in Polycrystalline NiTi And NiTiHf High Temperature Shape Memory Alloys*, in: vol Ph.D. dissertation, University of Central Florida, Orlando, 2012.
11. O. Benafan, R.D. Noebe, S.A. Padula II, D.J. Gaydosh, B.A. Lerch, A. Garg, G.S. Bigelow, K. An, R. Vaidyanathan, *Scr. Mater.* 68 (2013) 571-574.
12. A.P. Stebner, D.W. Brown, L.C. Brinson, *Acta Mater.* 61 (2013) 1944-1956.
13. O. Benafan, S.A. Padula II, R.D. Noebe, D.W. Brown, B. Clausen, R. Vaidyanathan, *Acta Mater.* <http://dx.doi.org/10.1016/j.actamat.2013.02.040> (2013).
14. ASTM Standard F2082-06, "Standard Test Method for Determination of Transformation Temperature of Nickel-Titanium Shape Memory Alloys by Bend and Free Recovery," 2010, ASTM International: West Conshohocken, PA, DOI: 10.1520/F2082-06, [www.astm.org](http://www.astm.org).
15. M.R. Daymond, M.A.M. Bourke, R.B.V. Dreele, B. Clausen, T. Lorentzen, *J. Appl. Phys.* 82 (1997) 1554-1562.
16. K. An, H. Skorpenske, A. Stoica, D. Ma, X.-L. Wang, E. Cakmak, *Metall. Mater. Trans. A* 42 (2011) 95-99.
17. X.-L. Wang, T.M. Holden, A.D. Stoica, K. An, H.D. Skorpenske, G.Q. Rennich, E.B. Iverson, A.B. Jones, *Mater. Sci. Forum* 652 (2012) 105-110.

18. K. An, X.-L. Wang, A.D. Stoica, Vulcan Data Reduction and Interactive Visualization Software (VDRIVE), <http://www.ornl.gov/~k6e/VDRIVE/> (2010).
19. S. Rajagopalan, A.L. Little, M.A.M. Bourke, R. Vaidyanathan, Appl. Phys. Lett. 86 (2005) 081901.
20. M.F.-X. Wagner, W. Windl, Acta Mater. 56 (2008) 6232-6245.
21. H. Sehitoglu, X.Y. Zhang, Y.I. Chumlyakov, I. Karaman, K. Gall, and H.J. Maier (Eds.), Observations on Stress-Induced Transformations in NiTi alloys, Hong Kong, 2002, p. 103-109.



REPORT DOCUMENTATION PAGE			Form Approved OMB No. 0704-0188		
<p>The public reporting burden for this collection of information is estimated to average 1 hour per response, including the time for reviewing instructions, searching existing data sources, gathering and maintaining the data needed, and completing and reviewing the collection of information. Send comments regarding this burden estimate or any other aspect of this collection of information, including suggestions for reducing this burden, to Department of Defense, Washington Headquarters Services, Directorate for Information Operations and Reports (0704-0188), 1215 Jefferson Davis Highway, Suite 1204, Arlington, VA 22202-4302. Respondents should be aware that notwithstanding any other provision of law, no person shall be subject to any penalty for failing to comply with a collection of information if it does not display a currently valid OMB control number.</p> <p>PLEASE DO NOT RETURN YOUR FORM TO THE ABOVE ADDRESS.</p>					
1. REPORT DATE (DD-MM-YYYY) 01-06-2013		2. REPORT TYPE Technical Memorandum		3. DATES COVERED (From - To)	
4. TITLE AND SUBTITLE Macroscopic and Microstructural Aspects of the Transformation Behavior in a Polycrystalline NiTi Shape Memory Alloy			5a. CONTRACT NUMBER		
			5b. GRANT NUMBER		
			5c. PROGRAM ELEMENT NUMBER		
6. AUTHOR(S) Benafan, Othmane; Noebe, Ronald, D.; Padula, Santo, A., II; Lerch, Bradley, A.; Bigelow, Glen, S.; Gaydosh, Darrell, J.; Garg, Anita; An, Ke; Vaidyanathan, Raj			5d. PROJECT NUMBER		
			5e. TASK NUMBER		
			5f. WORK UNIT NUMBER WBS 794072.02.03.03.01		
7. PERFORMING ORGANIZATION NAME(S) AND ADDRESS(ES) National Aeronautics and Space Administration John H. Glenn Research Center at Lewis Field Cleveland, Ohio 44135-3191			8. PERFORMING ORGANIZATION REPORT NUMBER E-18681		
9. SPONSORING/MONITORING AGENCY NAME(S) AND ADDRESS(ES) National Aeronautics and Space Administration Washington, DC 20546-0001			10. SPONSORING/MONITOR'S ACRONYM(S) NASA		
			11. SPONSORING/MONITORING REPORT NUMBER NASA/TM-2013-217878		
12. DISTRIBUTION/AVAILABILITY STATEMENT Unclassified-Unlimited Subject Categories: 37 and 32 Available electronically at <a href="http://www.sti.nasa.gov">http://www.sti.nasa.gov</a> This publication is available from the NASA Center for AeroSpace Information, 443-757-5802					
13. SUPPLEMENTARY NOTES					
14. ABSTRACT The mechanical and microstructural behavior of a polycrystalline Ni <sub>49.9</sub> Ti <sub>50.1</sub> (at.%) shape memory alloy was investigated as a function of temperature around the transformation regime. The bulk macroscopic responses, measured using ex situ tensile deformation and impulse excitation tests, were compared to the microstructural evolution captured using in situ neutron diffraction. The onset stress for inelastic deformation and dynamic Young's modulus were found to decrease with temperature, in the martensite regime, reaching a significant minimum at approximately 80 °C followed by an increase in both properties, attributed to the martensite to austenite transformation. The initial decrease in material compliance during heating affected the ease with which martensite reorientation and detwinning could occur, ultimately impacting the stress for inelastic deformation prior to the start of the reverse transformation.					
15. SUBJECT TERMS Mechanical engineering; Metals and metallic materials					
16. SECURITY CLASSIFICATION OF:			17. LIMITATION OF ABSTRACT	18. NUMBER OF PAGES 18	19a. NAME OF RESPONSIBLE PERSON
a. REPORT U	b. ABSTRACT U	c. THIS PAGE U			STI Help Desk (email:help@sti.nasa.gov)
					19b. TELEPHONE NUMBER (include area code) 443-757-5802



